ADVANCED ENGINEERING MATERIALS
www.aem-journal.com

Production of Metallic Foam Precursors Using Current-Activated Pressure-Assisted Densification

*Tillmann Robert Neu, Paul Hans Kamm, and Francisco García-Moreno**

The production of metallic foams is influenced by many aspects. Among other factors, compaction plays an important role in the powder metallurgical production of foamable precursors. A powder compaction metallurgical method, known as current-activated pressure-assisted densification (CAPAD), is applied to enhance the compaction of metal foam precursors. This method improves precursor quality by achieving higher density, lower electrical resistivity, and more uniform pore nucleation in the resulting foams. Changes in the microstructure, constituents' distribution, and their influence on the foam nucleation and expansion behavior are investigated. Compared to traditional uniaxial hot pressing (UHP) methods, CAPAD operates at significantly lower pressures than UHP, reducing energy consumption and processing time. The reduced operational demands and improved material properties highlight CAPAD's potential as a cost-effective and efficient alternative to conventional compaction techniques.

1. Introduction

The production of a metal foam via the powder metallurgical route is a two-step process. First, a precursor is made from powders, which is then foamed in a second step by heating it above the solidus temperature of the alloy composition. The compaction of the powders can be achieved by any technique that ensures a metal matrix without significant open porosity.[1] Such compaction can be accomplished by different methods such as hot uniaxial or isostatic pressing, extrusion, or powder rolling.[2] Each of these methods has its own advantages in certain areas, e.g., the highest throughput can be achieved by extrusion and rolling. Foamable precursors can also be produced by more exotic methods such as thixocasting,[3] accumulative roll-bonding,[4] friction stirring[5] or the Foamgrip[6] respectively. Foamcarp[7] process. However, all of them had a marginal volume outcome.

A main challenge in the metal foam production is to produce them with homogeneous structures, which are required, for e.g., to provide better thermal properties[8] or mechanical performance.[9] In order to achieve high expansion and homogeneous pore size distribution, the most critical step is the compaction of the precursor, which should result in a dense[10] and gas-tight matrix. In addition, other parameters such as alloy composition, powder size, shape, and condition[11] as well as parameters related to the compaction method, temperature, time, and applied pressure are also important.[1] Improvement of precursor compaction can also be achieved by compaction under vacuum[12] or by adding plasticizers such as Sn additives to Al foam precursors.[13] Spark plasma sintering (SPS) is a recognized method for rapid powder sintering with short sintering times, which is accelerated by particle surface activation and increased diffusion.[14] In SPS, an external pressure and an electric field with a usually pulsed DC current are applied simultaneously to promote the densification of the powder compacts into a dense body.[15] In contrast to the external heating produced by uniaxial or isostatic hot pressing, SPS allows an electrical current to pass through the conductive die and the powder so that the sample is heated from both the outside and the inside. SPS is known to promote electro migration, increasing atomic diffusion and intergranular metallic bonding.[16] SPS is also used in a variety of ways to produce porous materials, e.g., when sintering powders around spacers that are replaced in a subsequent step.[17]

Current-activated pressure-assisted densification (CAPAD) is essentially a uniaxial hot pressing (UHP) method in which the heat is generated internally by a constant high DC current conducted through the system punches.[18] CAPAD is applied to compact, e.g., ceramic powders.[19] Similar to SPS, heat is generated from the outside and inside, or only from the inside, by using an insulated die. The heat is generated where the resistivity is higher, i.e., at the powder particle contacts. CAPAD and SPS are essentially the same process, but SPS is usually applied under vacuum, with a graphite die and pulsed DC current, leading to sparks during the sintering process.

The motivation for this work is to use CAPAD to effectively generate the heat for compaction exactly where it is needed, namely at the contacts of the metal powder particles. This is

T. R. Neu, P. H. Kamm, F. García-Moreno
Institute of Materials Science and Technology
Technische Universität Berlin
Hardenbergstr. 36, 10623 Berlin, Germany
E-mail: garcia-moreno@helmholtz-berlin.de

T. R. Neu, P. H. Kamm, F. García-Moreno
Institute of Applied Materials
Helmholtz-Zentrum Berlin für Materialien und Energie
Hahn-Meitner-Platz 1, 14109 Berlin, Germany

The ORCID identification number(s) for the author(s) of this article can be found under https://doi.org/10.1002/adem.202501794.

DOI: 10.1002/adem.202501794

precisely the point at which a good metallic bond between the powder particles must be achieved. We selected CAPAD as the compaction process, as it better describes our experimental setup, with a steel die and continuous current. CAPAD saves time and energy as the heat is generated quickly and precisely where it is needed and not on the entire pressing tool, preserving the deterioration of the tooling. Especially when compacting foamable metallic precursors, it is very important to keep the overall temperature and specially around the blowing agent particles, usually TiH_2,[20,21] as low as possible to avoid their premature decomposition, but at the same time obtaining a gas-tight and dense precursor. SPS is not appropriate for our purpose, as too high local temperatures are produced for a short time interval, which will deteriorate our blowing agent. This is why we compare CAPAD with the standard and established compaction method UHP.

2. Experimental Section

2.1. Precursor Materials

The commercially relevant AlSi8Mg4 (in wt%) foamable composition with the addition of 0.25 wt% of TiH_2 as a blowing agent was selected for the foaming experiments.[22] Aluminum (AMG Alpoco UK Ltd., 99.7% pure, $D_{50} = 51\,\mu m$), silicon (Elkem AS, 97.5% pure, $D_{50} = 26\,\mu m$), pre-alloyed AlMg50 (in wt%) (Possehl Erzkontor GmbH, 99.5% pure, $D_{50} = 85\,\mu m$), and TiH_2 (Chemetall GmbH, Grade N, 98.8% pure, $D_{50} = 14\,\mu m$) powders were used. The TiH_2 powder was heat-treated at 480 °C for 180 min in air, delaying the hydrogen release range to higher temperatures to optimize the foaming performance of the selected alloy.[20,23] The powders were mixed in a tumbling mixer for 20 min and introduced into the corresponding die, being then ready for compaction.

2.2. Uniaxial Hot Compaction

Uniaxial hot compaction was one of the standard processes for compacting powders.[2] The powder was filled into a mold with the desired shape, sealed with a plunger, and then pressed. High pressures can easily be achieved due to the generally small quantities of powder or the small dimensions of the mold. For comparison purposes, conventional UHP using a hardened hot-worked steel die and a heating belt, as shown elsewhere,[1] was conducted. 5 g of the powder mixture was filled into a hollow cylinder made of hardened hot-work tool steel with an internal diameter of 15 mm and enclosed by two punches. All surfaces were lubricated with the MoS_2-based lubricant Molykote D321R (Dow Corning Inc.). Compaction was achieved by first cold-pressing the powder for 10 s at 300 MPa and room temperature using a hydraulic press (400 kN, Dema Vertriebs GmbH), then heating up to 400 °C with a resistive heating sleeve, which was placed around the cylinder. Subsequently, pressing for 15 min at 400 °C and finally unloading the press, removing the die, and quenching it.

2.3. The CAPAD Method

The precursor preparation was performed by the CAPAD method.[18] The applied setup configurations (low and high resistance die) are described in **Figure 1**. For conducting CAPAD (current flowing through the powders and die in parallel), the die was made of stainless steel with an inner diameter of 15 mm. For insulating CAPAD (current flowing only through the powders) an insulating aluminum oxide tube (inner diameter of 15 mm; wall thickness of 2.5 mm) placed in a steel jacket was used as a die. Force was applied with a uniaxial press (400 kN, Holzmann Maschinen GmbH, Austria). The schematic electrical circuit is shown in Figure 1b.

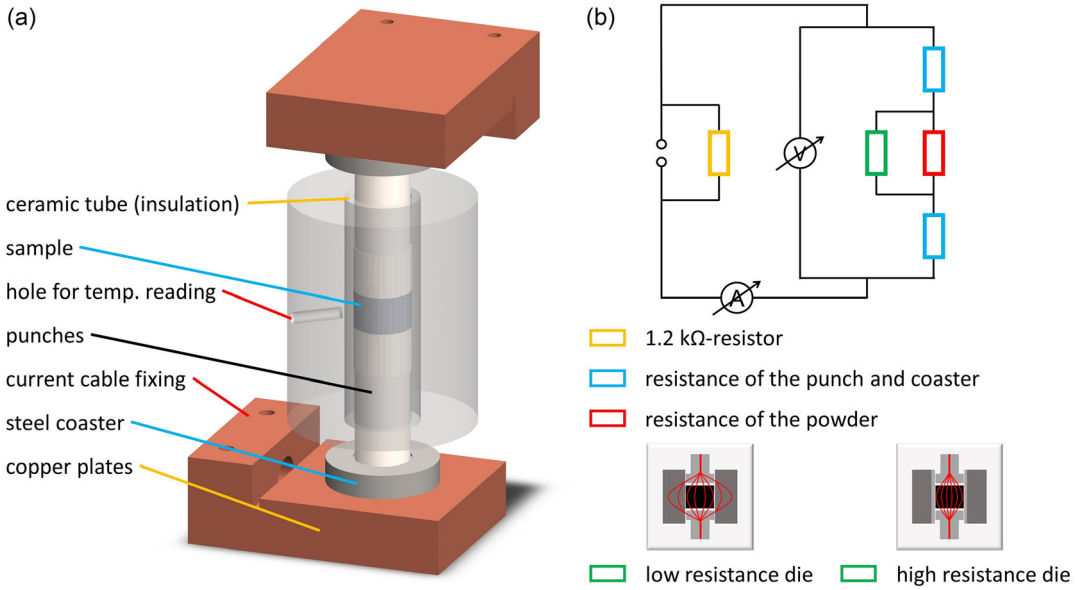

Figure 1. a) Main components of the pressing tool and b) schematic electrical circuit diagram and current paths through die and powder of the different CAPAD setups.

For the compaction process, the die was filled with 5 g of the powder blend and closed with matching punches. The current connection was realized via two copper plates, in which 120 mm^2 cables were clamped. In order not to damage the soft copper plates during pressing, a coaster made of steel was added between the punch and the copper plate. Finally, the whole construction was electrically insulated from the press. Power was supplied by two parallel RST-10 000 power supplies (Mean Well Enterprises Co., Ltd, Taiwan). A maximum power of 3.6 kW, i.e., a maximum current of 720 A with a voltage limited to 5 V, was applied. The current flow was determined by the resistance of the various conductive components, i.e., the powders, cables, dies, and punches, see Figure S1, Supporting Information.

The CAPAD compaction process was performed in the following way: 1) After the die was filled with powder and closed with the punches, the entire assembly was installed in the press, aligned in the pressing direction, and pressed with ≈80% of the compaction pressure. 2) Then the current flow was activated for 15 min, and the pressing pressure increased to 100%. The temperature of the die/steel jacket was measured through an aperture drilled near the sample, as shown in Figure 1. The temperature of the sample may differ from the temperature of the die, depending on where it was generated. The pressing force was adjusted and kept constant manually, with a deviation of about ±2 kN. 3) After switching off the current, the press was unloaded, the die with the sample and punches removed, and quenched in water.

A schematic representation of the particle arrangement and DC current flow inside the die is shown in **Figure 2**. Figure 2a represents the loose powders inside the die with a low bulk density before pressing, Figure 2b shows that after pressing, the density increases, and the oxide layers (blue lines around the particles) covering the powder particles break up first at these contact points.[24] This initial mechanical compaction of the powders was required to create a current path with sufficient conductivity to allow for high current flow at low voltages. Figure 2c indicates the possible current path through the die as red dashed lines (in the case of a conductive die) and through the particles as continuous red lines. The current follows the path of least resistance through the particles inside instead of across their surface, as we apply a constant current instead of a pulsed current, as with the SPS, which leads to the skin effect. The current was also forced to percolate between particles to avoid cavities. The red dots indicate the contact points between the particles, i.e., the points with the highest resistance. It was assumed that, similar to SPS, higher temperatures appear at the contact points caused by Joule heating,[15] which decreases sintering time and promotes diffusion by electromigration.[24]

2.4. Electrical Resistivity

The specific electrical resistivity of a precursor can be an indicator of the degree of metallic bonding between the sintered particles. A four-point contact method was used following Equation (1). For each measurement, the voltage U was measured at four different currents in the range of 1.5–3 A. The sample was contacted along a line at four contact points, each separated by 3 mm. The factor F_d corrects the influence between sample thickness d and distance between the measuring points, and F_l the influence of the lateral extent of the sample with the lateral expansion of the sample w and the distance between the contacts s according to.[25]

$$\rho_{el} = \frac{U}{I} \cdot \frac{\pi}{\ln 2} \cdot d \cdot F_d \cdot F_l \tag{1}$$

$$\text{with } F_d = \frac{ln2}{ln\left(\frac{sinhyp(d/s)}{sinhyp(d/2s)}\right)} \tag{2}$$

$$\text{and } F_l = \frac{ln2}{ln2 + ln\left(\frac{(w/2)^2+3}{(w/2)^2-3}\right)} \tag{3}$$

2.5. Metallographic Analyses

3.5 mm-thick slices were cut from the resulting compacted precursors for density measurements via the Archimedes method. The relative density was determined by the ratio of measured to the theoretical density of the alloy, the latter being taken from the calculation of Helwig et al.[1] and corresponding to 2.632 g cm^{-3}. This value was an approximation taking 0.7 wt% of alumina into account for powders heat-treated in a hot pressing die.[26] The sample surfaces were mechanically ground using 120–2400 grit silicon carbide paper, polished successively with 3 and 1 µm diamond paste, and finally polished with a SiO_2 suspension. Light microscopic images were taken with an Axioplan 2 microscope

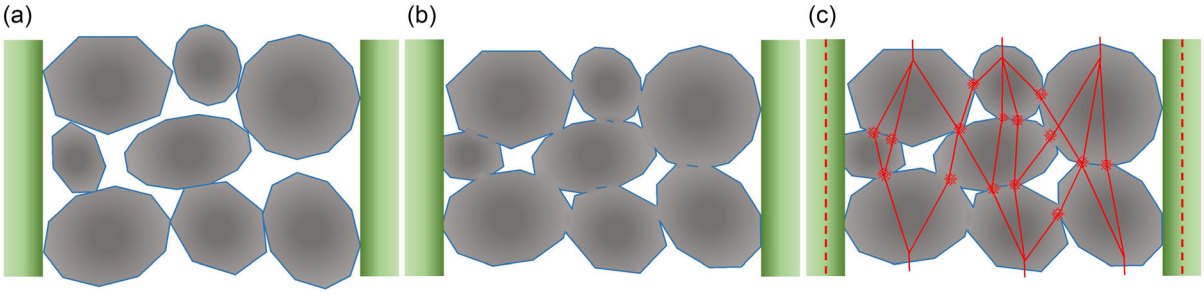

Figure 2. Schematic representation of powder particle alignment inside a mold during CAPAD: a) loose powders, b) after cold compaction, and c) possible current path (red lines) and points of highest resistance between the particles. For the conducting die, the dashed lines also apply, adapted for DC current from Cavaliere et al.[15]

(Carl Zeiss AG, Germany). Scanning electron microscopy (SEM) images and energy dispersive X-ray analysis (EDX) were obtained with a GEMINI LEO 1530 (Carl Zeiss AG, Germany), operated at a 7 kV accelerating voltage. A rough estimation of the number of phases was performed by image analysis of the microscopic images, averaged over 3 different images.

2.6. X-Ray Imaging of the Metal Foaming Process

The samples were foamed on a ceramic heating plate under air, and the liquid foam evolution, the pore structure, and the foam expansion profiles were observed and quantified in situ in an X-ray imaging system. The radioscopy setup consists of a microfocus X-ray source with a tungsten target operated at 100 kV and 100 µA, and a 2240 × 2368 pixel flat panel detector, both from Hamamatsu, Japan, described in detail elsewhere.[27] The temperature was controlled by a PID controller (CAL 3300, Cal Controls Ltd, UK) and measured by a thermocouple embedded directly in the heating plate beneath the sample. The real temperature of the sample during foaming was calibrated in advance by an additional thermocouple inside a dummy sample at the foaming position. The same X-ray imaging system also allowed for the record of post-processing tomograms of the resulting solidified foams by replacing the heating plate with a tomographic rotation stage (HUBER GmbH, Germany). For that purpose, 1000 projections over 360° with an exposure time of 2 s per projection were recorded, from which tomograms were reconstructed with the commercial software Octopus 8.8 (Inside Matters, Belgium). 3D visualization and quantitative evaluation were done with the commercial software Avizo (Thermo Fisher, USA).

3. Results

3.1. Dependence of Compacting Pressure

Powders of the composition AlSi8Mg4 (in wt%) with the addition of 0.25 wt% of TiH_2 as a blowing agent were mixed and compacted under different conditions by standard UHP with a resistive heating belt, conducting and insulating CAPAD. The relative densities of the compacts and their electrical resistivity for different compacting pressures are plotted in **Figure 3**. It can be observed that even at low compacting pressures of 28 MPa, both CAPAD variants exhibit high relative densities of the resulting precursors of ≈99%, which quickly rise to 99.5% of the theoretical value at 57 MPa for insulating CAPAD (Figure 3a). With UHP, the relative density of the precursor seems to slowly converge against the presumed upper limit of 100% with increasing pressure, but only exhibiting a relative density of 95.2% at 115 MPa, 97.8% at 170 MPa, and 98.8% at 230 MPa. At the lowest compaction pressure of 57 MPa for UHP, they only achieve a value of 88.9 ± 0.6%. Even increasing the heating temperature of UHP to 500 °C at 57 MPa in an additional experiment only leads to 93.5 ± 0.6% rel. density and 5.14 ± 0.14 µΩcm, both significantly lower than when applying CAPAD.

The electrical resistivity decreases with pressure for all conditions and saturates at 4.6 µΩcm for pressures in the range of 170−288 MPa with UHP. With CAPAD, the electrical resistivity is already <4.5 µΩcm at the lowest applied pressure of 28 MPa and therefore lower than for UHP at the highest available pressure of 288 MPa.

3.2. Microstructure of the Precursors

Based on the microstructure analyses, we can determine that in UHP samples, Si, Mg_2Si, and AlMg particles with both beta and gamma phases are still visible, as shown in **Figure 4**a. On the opposite, for insulating CAPAD (Figure 4b) and conducting CAPAD (Figure 4c), only Si and Mg_2Si particles can be identified in the matrix together with a large number of small grain boundary precipitations. Further, areas with higher Mg content (but within the solubility of Al) are detectable for CAPAD (Figure 4b,c), as shown by the EDX analysis in **Figure 5**. There, we can observe that the Mg_2Si regions in CAPAD precursors are not evenly distributed over the whole matrix. The detailed EDX analysis in Figure 5 revealed that the Mg-containing areas are mainly composed of the Mg_2Si phase. As a rough indicative comparison analysis of

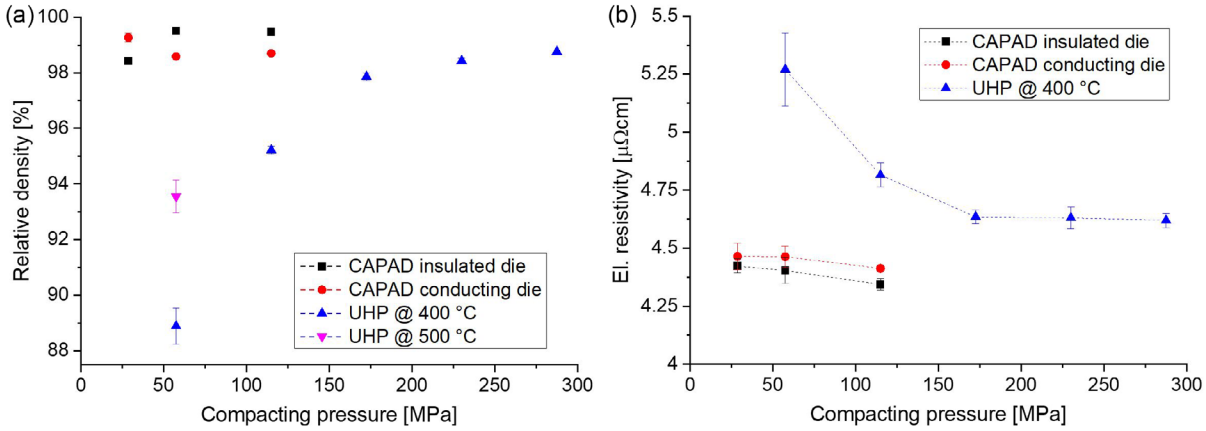

Figure 3. a) Relative density and b) electrical resistivity of the compacted precursors over the compacting pressure for conducting and insulating CAPAD compared with standard uniaxial hot compaction with an external heater. There are at least 3 samples per condition. Some error bars are too small to be displayed.

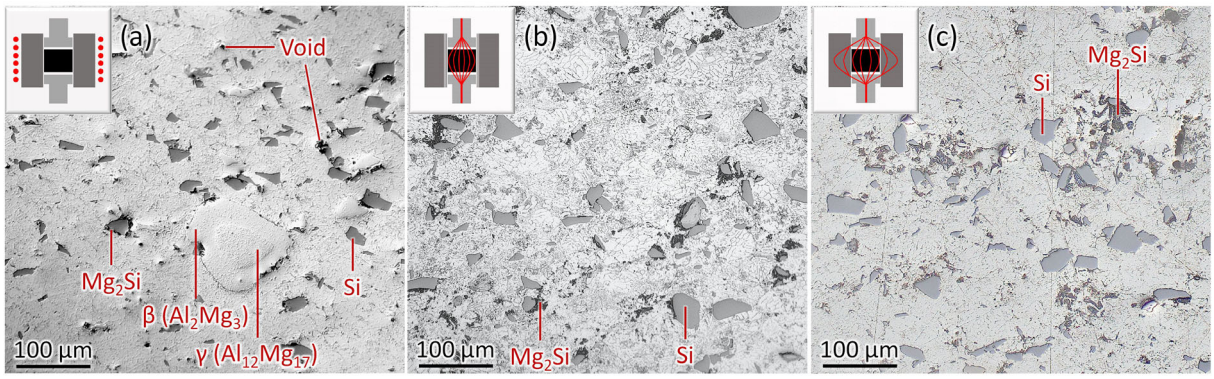

Figure 4. Metallographic images of the precursors compacted with 115 MPa and heated by a) UHP, b) insulating CAPAD, and c) conducting CAPAD. Main phases are labeled exemplarily with regard to their composition. The insets denote schematically the corresponding heating and compaction method.

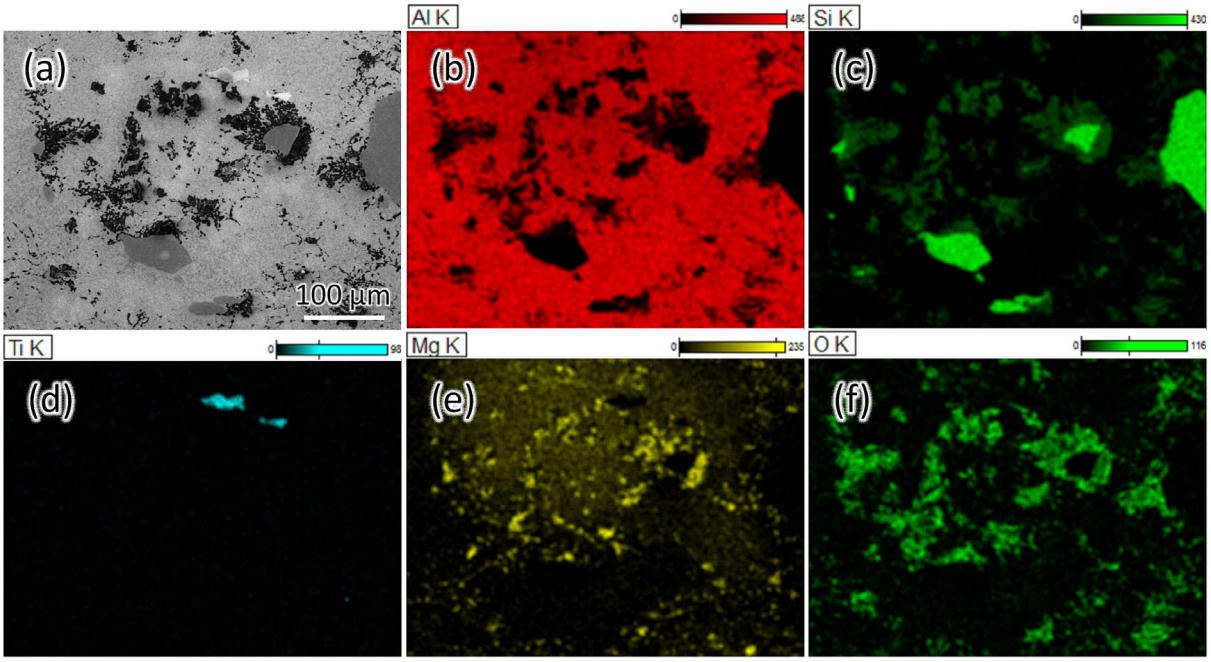

Figure 5. a) SEM image and EDX-MAP of a precursor produced by an insulating CAPAD die with 115 MPa showing the distribution of b) Al, c) Si, d) Ti, e) Mg, and f) oxygen. AlMg50 particles are to a certain extent dissolved in the Al matrix (yellow background in e), but still localized in small agglomerates of Mg_2Si particles (yellow spots in e) and light green spots in (c).

the light microscopic representative images in Figure 4 indicated more than two times more Mg_2Si for insulating CAPAD and nearly two times more for CAPAD conducting compared to UHP, although this is only an estimate, as the actual phase fractions cannot be determined accurately from 2D sections, as these provide only limited spatial information about the 3D phase distribution. Existing residual porosity according to the relative density measurements is hardly detectable in metallographic images because of the smearing effect of polishing, though some voids can be observed in the case of UHP (see Figure 4a). A more detailed microscopic and EDX analysis of the phases involved in pore nucleation was presented by Kamm et al.[28,29]

3.3. Foaming Behavior

At medium compaction pressures of 115 MPa, only precursors compacted using the CAPAD method allow foaming at the alloy's standard foaming temperature of 630–650 °C,[1] as can be observed in **Figure 6**b,c. In contrast, the precursor compacted with UHP does not foam at all at this pressure and just experiences thermal expansion (Figure 6a). The expansion and foam structures corresponding to the precursors produced with CAPAD are reasonable, as can be observed by selected X-ray images extracted from radioscopic sequences obtained in situ during the foaming process and shown in Figure 6b, c. In case of conducting CAPAD, large cracks

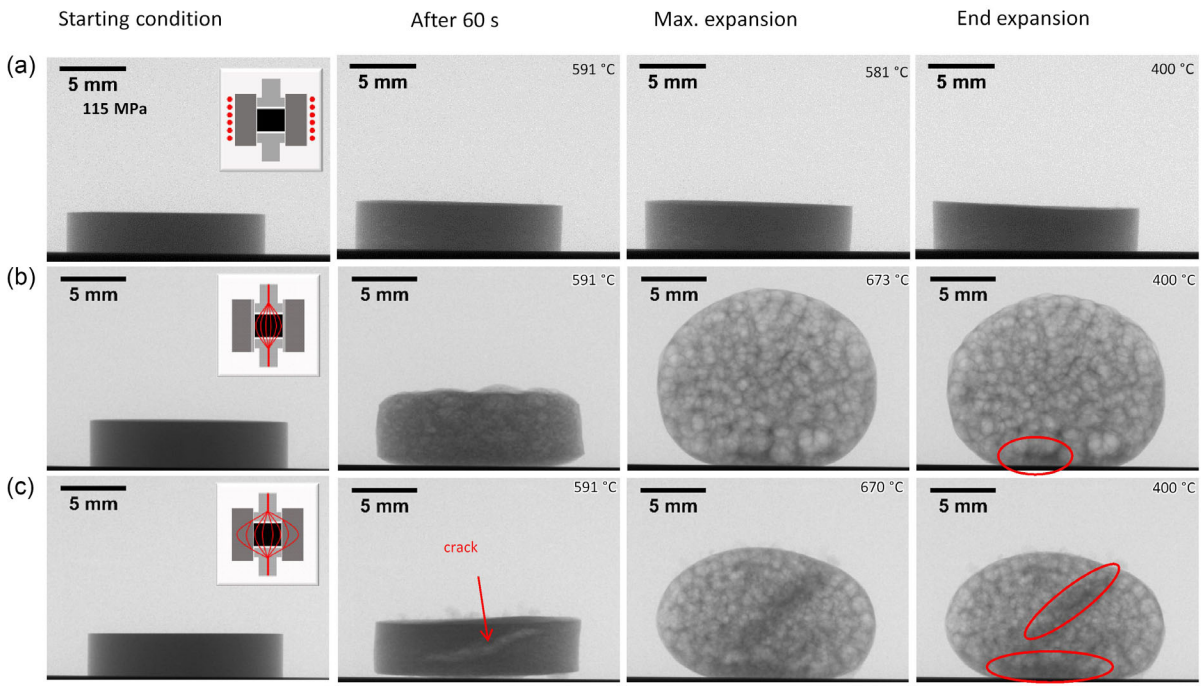

Figure 6. Selected X-ray radiographies during foaming of precursors at 650 °C extracted from the in situ radioscopic sequences at different stadiums (precursor at RT, after 60 s heating, maximal expansion, end expansion) for precursors compacted with the same pressure (115 MPa) during 15 min but with different uniaxial compaction methods: a) UHP, b) insulating CAPAD, and c) conducting CAPAD. Sample temperature is given in the upper right corner. The insets denote schematically the corresponding heating and compaction method. A crack in the precursor is marked with a red arrow, and denser foam regions are marked with red ovals.

were observed in 66% of the cases after 60 s of foaming, shown with a red arrow in Figure 6c. Occasionally, a few small dark areas (marked with red ovals in Figure 6) can be observed, which correspond to denser regions caused by a slight gravity-induced drainage or cracks in the precursor at early foaming stages.

Figure 7 shows similar X-ray images of the evolution of the foaming procedure, like Figure 6, but for precursors compacted with 230 MPa in the case of UHP (Figure 7a) and with 28 MPa in the case of CAPAD (Figure 7b,c). The precursor compacted with UHP foams very well but shows cracks that grow to big pores (indicated with red arrows in Figure 7a),[24] while the samples made with CAPAD result in slightly lower expansion and larger or similar pores at the end of the process, as can be observed in Figure 7b,c, respectively. The insulated die (insulating CAPAD) shows very homogeneous nucleation and pore structure (Figure 7b). These results show that using the CAPAD method, an order of magnitude less compacting pressure than for standard UHP can be used to reach acceptable expansions and structures.

A more detailed and quantitative comparison of the foamability of the precursors is shown in **Figure 8**, in which the maximum cross-sectional expansion of the foam is plotted against the applied pressure. Precursors compacted using standard UHP can only be foamed at compaction pressures above ≈150 MPa, but then have a higher expansion capability (≈350% area expansion) than the samples compacted with CAPAD (200−250% area expansion).

Tomograms of the foams were analyzed to better assess the homogeneity of their pore structure. When comparing whole samples, the expansion of the foam must be considered. For this purpose, the full width at half maximum (FWHM) of the pore size distributions was plotted against the mean pore equivalent diameter, normalized to the total sample volume. The normalization makes it possible to find trends for different heating modes, as can be seen in **Figure 9**. The pores of foamed precursors produced with UHP related to the foam volume are generally smaller than those with CAPAD, but less homogeneously distributed, which is reflected in a larger FWHM. Applied pressure does not show a clear trend, but with CAPAD, very low pressures show larger pores and wider size distributions in most cases.

4. Discussion

In the previous section, we were able to show that CAPAD can be successfully applied for the production of foamable metallic precursors at much lower pressure and more homogeneous pore structure than conventional UHP. In this section, we want to discuss the reasons for this behavior.

4.1. Precursor Compaction

Different factors influence a proper powder compaction following standard powder metallurgical production procedures. In general, the density of a powder compact can be increased through an increase of pressure, temperature, or time, while other factors

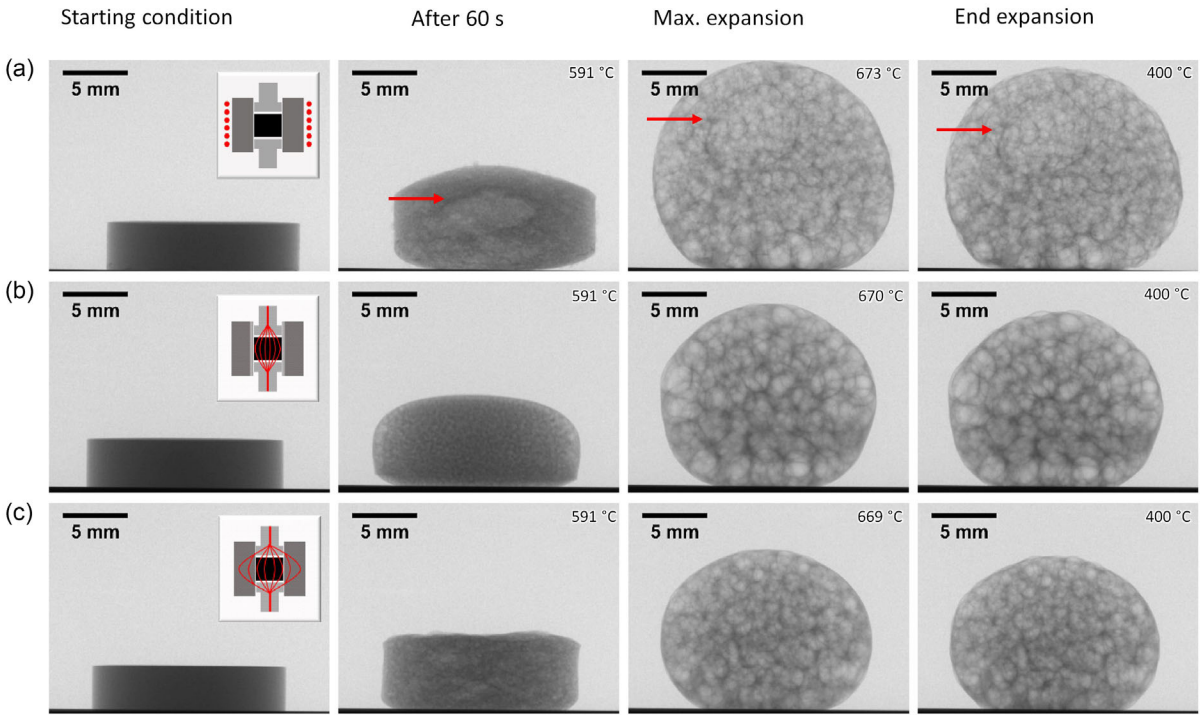

Figure 7. Selected X-ray radiographies during foaming of precursors extracted from the in situ radioscopic sequences at different stadiums (precursor at RT, after 60 s heating, maximal expansion, end expansion) for precursors compacted with different pressures during 15 min and with different uniaxial compaction methods. Sample temperature is given in the upper right corner. The insets denote schematically the corresponding heating and different compaction methods: a) UHP, b) insulating CAPAD, and c) conducting CAPAD. Sample temperature is given in the upper right corner. The insets denote schematically the corresponding heating and compaction method. A crack in the precursor and the corresponding large pore in the foam are marked with red arrows.

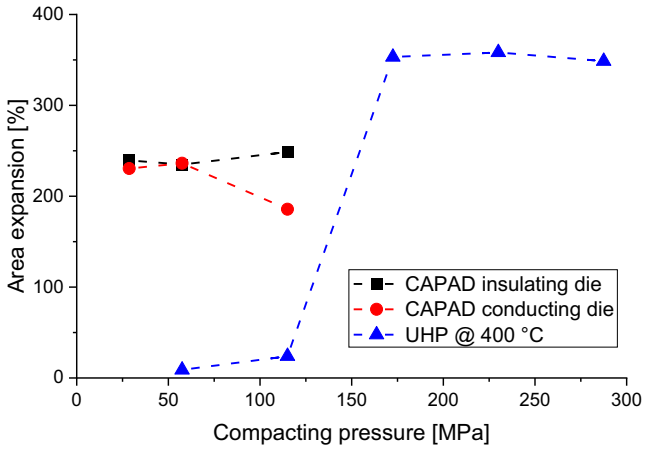

Figure 8. Cross-sectional foam maximal area expansion over compacting pressure for precursors prepared with CAPAD and uniaxial hot compaction with heating belt at 400 °C.

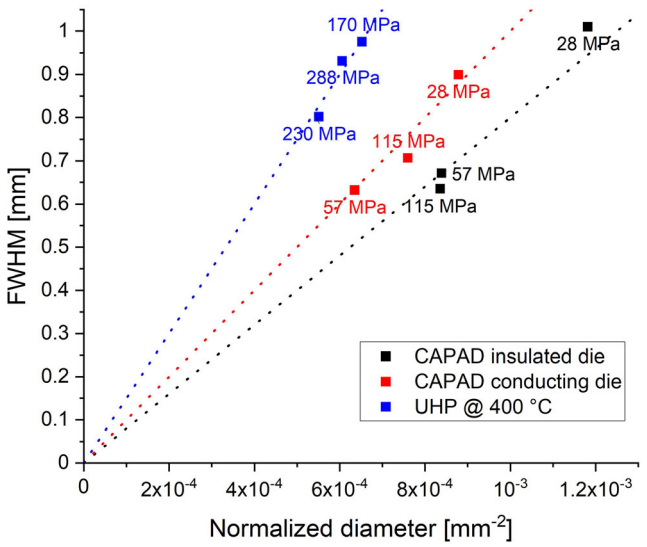

Figure 9. Comparison of characteristic values - FWHM of the pore size distributions over mean pore equivalent diameter normalized by the total volume.

such as powder size, powder oxide content, compaction atmosphere, etc., also influence the process.[30] Current assistance is an additional parameter as applied in SPS.[14] CAPAD is not as common as SPS, the main difference being that the current flow is not pulsed, but a high, constant direct current.

While high density and good mechanical properties are the aim in standard UHC and SPS powder metallurgy compaction processes, the former is more important in the production of metal foam precursors, while the mechanical performance of the precursors is irrelevant, as they have to be foamed in a following step. A high density of precursors and metallic bonding of

the powder particles to avoid blowing agent gas losses during heating are crucial for a good metal foaming result based on homogeneous bubble nucleation and effective utilization of the expanding gas. If the precursor is not sufficiently gas-tight, part of the evolving gas escapes into the surrounding atmosphere due to the residual porosity and cannot contribute to foaming, which leads to lower expansions. Helwig et al. showed that for the common AlSi8Mg4 foamable alloy precursor, pressure, temperature, and time influence foaming, and a minimum precursor density of 97.5% is required to achieve acceptable foaming expansion. Best foaming results can be achieved between 97.5%-99%.[1] As the blowing agent TiH_2 normally used for foaming aluminum alloys starts to release gas at around 400 °C, the compaction temperature applying the UHC method should be kept as close to this value as possible.[20] Furthermore, it was found that even the heating rate applied during the compaction of the pre-product influences the foaming, suggesting that the kinetics of formation of the low-melting phases involved in nucleation play an important role.[31]

Figure 3a shows that conventional UHP reaches only densities >97.5% for pressures of 170 MPa or higher of the precursors, while CAPAD reaches densities of >98% even at the lowest tested pressure of 28 MPa, showing a considerable advantage from CAPAD compared to conventional UHP, especially at low pressures. CAPAD achieves higher density values at 400 °C compared to UHP at the same pressure, even if the temperature is increased to 500 °C by UHC. The latter has a detrimental effect on the foaming process due to the limitations caused by the premature decomposition of the blowing agent. The improved electrical conductivity of the precursor obtained by CAPAD compaction, as shown in Figure 3b, is an indicator of higher density and better metal bonding between single particles, enhanced by the current conducting paths through the powders, similar to what is known from SPS.[24] The reason is an initial high local temperature at the particle contacting points due to a high resistance and probably enhanced by electromigration similar to SPS,[32] that leads to diffusion, neck formation, and sintering.[15] In general, the insulating CAPAD method shows the best compaction (higher density, lower el. resistivity) among the precursors, as more current has to flow through the metallic powders instead of through the die.

We also observe an anticorrelation behavior between density and electrical resistivity in dependence on the compacting pressure for both methods, as the contact area increases with density. In addition, the resistivity of CAPAD precursors is lower because not only diffusion but also current influences mass transfer, which contributes to metallic contact through the formation of intermetallic phases and densification.[33] The influence of current on mass transport can be manifested through the electron wind effect (electromigration),[34] or by an increase in point defect,[35] or by a decrease in the activation of migration of the defects.[36] In this sense, CAPAD insulation achieves higher densities and a lower resistivity, as can be seen in Figure 3b, since the entire current flows through the powder and not partially through the die.

The resistance of the powder is quite high at the beginning, as the bulk density of the powder is still low before compaction, with a small number of contact points, and fresh Al powder particles also have a thin Al oxide layer with a higher resistance. In the course of compaction, the density increases up to the point at which the powder begins to deform and the oxide layer breaks off, as a result of which the resistance decreases quite quickly, as can be seen in Figure S1, Supporting Information. When resistivity lowers, the current effect can increase with time, as the total current through the sample increases with time. As aluminum is a good electrical conductor and the cross-sectional area of the powder sample is considerably larger than the cross-section of the copper cables, during the process, its resistance becomes lower than that of the cables.

The temperature measured during the compaction process is an integral value measured at a similar position in both cases, as close to the sample as possible (see Figure 1). There is a difference between the temperature evolution depending on the configuration chosen (conducting or insulating die) and also on the pressure applied. The temperature evolution on the samples for conducting CAPAD is up to 100 K higher than for insulating CAPAD, see Figure S2, Supporting Information. We assume that the temperature difference between the insulating and conducting configuration results from the parallel arrangement of the two current paths, that of the powder and that of the die, last being absent in the case of the insulating die. The additional heat produced in the die by conducting CAPAD results in a higher temperature at the sample. Further, lower compaction pressures lead to worse contact between the powder grains and higher resistivity, resulting in higher local temperatures. With insulating CAPAD, the latter only happens after almost 900 s at the lowest pressure of 28 MPa, i.e., at the very end of the process. Here, the powders are almost loose and have a small conductive cross-section. As the voltage is limited, more time is needed to sinter the first current paths, lower the resistance, and allow gradually the entire available current to flow through the sample. Despite lower temperatures during compression, insulating CAPAD leads to slightly denser and more conductive precursors than conducting CAPAD, see Figure 3.

One advantage of CAPAD in terms of better compaction performance compared to standard UHP is, that the main current paths can take place through the more conducting metallic powders of the matrix, in our case Al and Mg, or even through the AlMg50 particles, whose main phase is γ-$Mg_{12}Al_{17}$, rather than through the Si or TiH_2 blowing agent particles, which have a higher resistivity, as can be seen in **Table 1**. This is an important point, as the temperature of the blowing agent particles must be kept as low as possible to avoid their premature decomposition, as stated before, while a higher local temperature of the metallic matrix particles at their contact point, where the current passes, improves sintering. This effect disappears in the course of

Table 1. Electrical resistivity of the used phases as given in the literature.

Phase	ρ @ 20 °C [10^{-8} Ωm]	ρ @ 400 °C [10^{-8} Ωm]	Reference
Al	2.67	7.3	[44]
Mg	4.2	12.1	[44]
Si	5.8 10^4		[45]
	Depending on impurities		–
γ-$Mg_{12}Al_{17}$	29.6		[46]
$TiH_{1.75}$	86.2 (@50 °C)	126	[47]

compaction, as the density and metallic bonding of the particles increase, and the thermal conductivity improves, homogenizing the temperature distribution. Toward the end of the process, the temperature is then more homogeneous across the entire sample. As an example, the temperature difference between a particle–particle contact and the center of a good conducting particle is in the order of 1 mK for a copper particle with a radius of 50 mm and a contact radius of 5 mm.[32] The improved precursor densities achieved with CAPAD at low pressures can be explained in this sense.

In addition to the lower pressure required, consolidation with CAPAD takes only about 15 min compared to 40 min for the entire UHP process, see Figure S2, Supporting Information. If only the energy released between the punches is calculated without taking into account losses given by the cables, about 0.18 kWh is consumed to produce one sample, while UHP requires about 0.48 kWh to reach and maintain the same temperature in the mold (see **Table 2**).[37]

4.2. Microstructure

As diffusion through CAPAD is also enhanced by higher local temperature, we can observe that large AlMg50 particles are not detectable anymore in compacted precursors and Mg is mostly dissolved in the matrix or has formed Mg_2Si, in contrast to UHP, where former AlMg50 particles are still recognizable, with β- and γ-phases as shown in Figure 4. As known from the literature, AlMg particles play an important role in the nucleation of this alloy as adsorbed gas[29,38] and the early melting phase.[28] Mg_2Si regions in CAPAD precursors are not evenly distributed over the whole matrix, but there are still plenty of Mg-rich regions distributed in the matrix (Figure 5), which allow for homogeneously distributed low-melting nucleation areas as can be observed in Figure 6b. This fact may explain the more homogeneous nucleation of CAPAD, but also the overall lower expansion as a consequence of the lower amount of available AlMg regions due to the formation of more Mg_2Si particles compared to UHP. On the other hand, most Si particles appear to be intact in all compaction methods investigated here, as pure Si has a high melting point (1.414 °C) and a low diffusivity in Al.[39,40]

4.3. Foaming Process

The foaming process was observed in situ with X-ray radioscopic images (Figure 6). Compaction of the precursor with CAPAD at 115 MPa was sufficient for foaming, in contrast to standard compaction with UHP at the same pressure. The UHP precursor compacted at 400 °C and 115 MPa with a relative density of ≈97.5% does not foam at all (Figure 6a), as it obviously does not have sufficient density and gas tightness, but too much interconnected porosity.[1] In case of conducting CAPAD, large cracks were observed after 60 s of foaming in some cases, leading to gas losses and a reduced expansion of the whole sample. Further, such large cracks lead during foam evolution to a collapsed denser region and some liquid drainage at the bottom of the sample, visible, e.g., at the maximum or end expansion stadium in Figure 6c. But the foaming behavior of the rest of the precursor was good, indicating that these cracks were probably singular effects that can be avoided by further optimization of the process. We can clearly say that CAPAD enables the foaming of precursors with high density, which are obtained at significantly lower pressures compared to UHP.

Table 2. Energy savings.

Compaction method	UHP	CAPAD
	0.48 kWh	0.18 kWh

Figure 7 compares the foaming process of precursors compacted at the lowest possible pressure (28 MPa with CAPAD and 170 MPa with UHP). Precursors compacted with CAPAD expand more slowly (Figure 7, after 60 s) and less than those compacted with UHP (Figure 7, max. expansion), which is probably due to some gas loss due to higher local temperature, similar to the outgassing effect known from SPS.[41] In the case of insulating CAPAD, the early pore structure after 60 s and the final pore structure are the most homogeneous, which is important for a good mechanical performance.[42,43]

The quantitative foam expansion analysis extracted from the radioscopic images (Figure 8) clearly shows that precursors compacted with CAPAD in the pressure range 28–115 MPa can foam, while standard UHP compacted precursors require at least 170 MPa for foaming. The final foam expansion is not as high as with UHP, around 30% less than for UHP, but this could be an effect of slight gas losses due to the increased local temperature, and could be compensated with a slightly higher amount of blowing agent. The amount of blowing agent used in this work for all samples (0.25 wt% TiH_2) had previously been optimized in earlier work for the specific alloy AlSi8Mg4 (in wt%) and the UHP process, but was kept constant for comparison purposes. Higher foam expansion with CAPAD can be achieved by increasing the amount of blowing agent, and this will be investigated in future work. Not only is the maximum expansion the decisive quality criterion, but also the homogeneity of the cellular structure.[42] The foam pore sizes related to the foam expansion volume do not show a clear trend in dependence on the applied compaction pressure, but with CAPAD, very low pressures (e.g., 28 MPa) lead to larger pores and wider size distributions in most cases, as shown in Figure 9, indicating that the compaction pressure is not homogeneous and should not be reduced more.

Overall, the reduction in the required pressure achieved with CAPAD is a commercial advantage and opens up the possibility of cost reduction, as the need for high compaction pressures for large-scale production and large precursors is a disadvantage when it comes to making a breakthrough in metal foam products produced by powder metallurgy.

5. Conclusions

CAPAD, as an alternative powder metallurgical compaction method for metal foam precursors, was introduced. This method requires approximately one order of magnitude less compacting pressure compared to standard UHP. The insulating CAPAD exhibits better densification by achieving higher density and lower electrical resistance in the precursors, indicating a better metallic bonding of the precursors due to the additional effect of

current assistance, leading to more effective use of the blowing agent. The low-melting Mg-rich regions, which are responsible for nucleation, are more homogeneously distributed, resulting in more homogeneous pore nucleation leading to a more homogeneous pore structure, but less expansion of the resulting foams. Since CAPAD allows for faster consolidation at significantly lower pressures while consuming less energy than standard UHP, it offers significant cost-saving and scalability potential.

Supporting Information

Supporting Information is available from the Wiley Online Library or from the author.

Acknowledgements

The authors would like to thank Prof Banhart for the support of Dr Tillmann Neu's doctoral thesis.

Open Access funding enabled and organized by Projekt DEAL.

Conflict of Interest

The authors declare no conflict of interest.

Data Availability Statement

The data that support the findings of this study are available from the corresponding author upon reasonable request.

Keywords

current-activated pressure-assisted densification, metal foam, powder compaction, powder sintering

Received: July 7, 2025
Revised: October 10, 2025
Published online:

[1] H. M. Helwig, S. Hiller, F. Garcia-Moreno, J. Banhart, *Metall. Mater. Trans. B* **2009**, *40*, 755.
[2] J. Banhart, *Prog. Mater. Sci.* **2001**, *46*, 559.
[3] J. Weise, H. Stanzick, J. Banhart, *Cellular Metals: Manufacture, Properties, Applications* (Eds: N. A. F. J. Banhart, A. Mortensen), MIT, Berlin, Germany **2003**, p. 169.
[4] K. Kitazono, E. Sato, K. Kuribayashi, *Scripta Mater.* **2004**, *50*, 495.
[5] Y. Hangai, T. Utsunomiya, *Metall. Mater. Trans. A* **2009**, *40*, 275.
[6] V. Gergely, B. Clyne, *Adv. Eng. Mater.* **2000**, *2*, 175.
[7] V. Gergely, D. C. Curran, T. W. Clyne, *Compos. Sci. Technol.* **2003**, *63*, 2301.
[8] T. Fiedler, E. Solórzano, F. Garcia-Moreno, A. Öchsner, I. V. Belova, G. E. Murch, *Materialwiss. Werkstofftech.* **2009**, *40*, 139.
[9] T. R. Neu, P. H. Kamm, N. Von der Eltz, H.-W. Seeliger, J. Banhart, F. García-Moreno, *Mater. Sci. Eng., A* **2021**, *800*, 140260.
[10] A. R. Kennedy, *Powder Metall.* **2002**, *45*, 75.
[11] S. Asavavisithchai, A. R. Kennedy, *Adv. Eng. Mater.* **2006**, *8*, 810.
[12] C. Jiménez, F. Garcia-Moreno, M. Mukherjee, O. Goerke, J. Banhart, *Scripta Mater.* **2009**, *61*, 552.
[13] L. Y. Aguirre-Perales, I.-H. Jung, R. A. L. Drew, *Acta Mater.* **2012**, *60*, 759.
[14] V. Mamedov, *Powder Metall.* **2002**, *45*, 322.
[15] P. Cavaliere, B. Sadeghi, A. Shabani, *Spark Plasma Sintering Of Materials: Advances In Processing And Applications* (Ed: P. Cavaliere), Springer International Publishing, Cham **2019**.
[16] E. G. Grigoryev, E. A. Olevsky, *Scripta Mater.* **2012**, *66*, 662.
[17] D. V. Dudina, B. B. Bokhonov, E. A. Olevsky, *Materials* **2019**, *12*, 541.
[18] J. E. Garay, *Annu. Rev. Mater. Res.* **2010**, *40*, 445.
[19] E. Penilla, P. Sellappan, M. Duarte, A. Wieg, M. Wingert, J. Garay, *J. Mater. Res.* **2020**, *35*, 1.
[20] C. Jiménez, F. Garcia-Moreno, B. Pfretzschner, M. Klaus, M. Wollgarten, I. Zizak, G. Schumacher, M. Tovar, J. Banhart, *Acta Mater.* **2011**, *59*, 6318.
[21] C. Jiménez, F. Garcia-Moreno, A. Rack, R. Tucoulou, M. Klaus, B. Pfretzschner, T. Rack, P. Cloetens, J. Banhart, *Scripta Mater.* **2012**, *66*, 757.
[22] H. M. Helwig, F. Garcia-Moreno, J. Banhart, *J. Mater. Sci.* **2011**, *46*, 5227.
[23] B. Matijasevic, J. Banhart, *Scripta Mater.* **2006**, *54*, 503.
[24] J. Trapp, B. Kieback, *Powder Metall.* **2019**, *62*, 297.
[25] I. Miccoli, F. Edler, H. Pfnür, C. Tegenkamp, *J. Phys.: Condens. Matter* **2015**, *27*, 223201.
[26] S. Asavavisithchai, A. R. Kennedy, *Adv. Eng. Mater.* **2006**, *8*, 568.
[27] F. Garcia-Moreno, M. Fromme, J. Banhart, *Adv. Eng. Mater.* **2004**, *6*, 416.
[28] P. H. Kamm, T. R. Neu, F. García-Moreno, J. Banhart, *Acta Mater.* **2021**, *206*, 116583.
[29] K. Georgy, C. E. Jiménez, F. García-Moreno, M. Mukherjee, *J. Porous Mater.* **2025**, *32*, 935.
[30] J. Pickens, *J. Mater. Sci.* **1981**, *16*, 1437.
[31] T. Neu, B. Pfretzschner, F. García-Moreno, J. Banhart, *Metals* **2017**, *7*, 323.
[32] J. Trapp, B. Kieback, *J. Am. Ceram. Soc.* **2015**, *98*, 3547.
[33] Z. A. Munir, U. Anselmi-Tamburini, M. Ohyanagi, *J. Mater. Sci.* **2006**, *41*, 763.
[34] H. Huntington, A. Nowick, J. Burton, *Diffusion in solids: recent developments*, (Eds: A. S. Nowick, J. J. Burton), *6*, Academic Press, New York **1975**.
[35] P. Asoka-Kumar, M. Alatalo, V. J. Ghosh, A. C. Kruseman, B. Nielsen, K. G. Lynn, *Phys. Rev. Lett.* **1996**, *77*, 2097.
[36] J. E. Garay, S. C. Glade, U. Anselmi-Tamburini, P. Asoka-Kumar, Z. A. Munir, *Appl. Phys. Lett.* **2004**, *85*, 573.
[37] T. R. Neu, *Ph.D. Thesis*, Technische Universität, Berlin **2019**.
[38] K. Georgy, P. H. Kamm, T. R. Neu, M. Mukherjee, F. García-Moreno, *Mater. Charact.* **2025**, *219*, 114625.
[39] S.-I. Fujikawa, K.-I. Hirano, Y. Fukushima, *Metall. Trans. A* **1978**, *9*, 1811.
[40] E. Crossin, J.-Y. Yao, G. B. Schaffer, *Powder Metall.* **2007**, *50*, 354.
[41] A. S. Chua, M. Brochu, D. P. Bishop, *Powder Metall.* **2015**, *58*, 51.
[42] I. Jeon, T. Asahina, *Acta Mater.* **2005**, *53*, 3415.
[43] Y. P. Jeon, C. G. Kang, S. M. Lee, *J. Mater. Process. Technol.* **2009**, *209*, 435.
[44] C. J. Smithells, *Smithells Metals Reference Book*, Elsevier Butterworth-Heinemann, Amsterdam **2004**.
[45] F. G. Wick, *Phys. Rev. Series I* **1908**, *27*, 11.
[46] P. Donnadieu, S. Benrhaiem, C. Tassin, F. Volpi, J.-J. Blandin, *J. Alloys Compd.* **2017**, *702*, 626.
[47] M. Ito, D. Setoyama, J. Matsunaga, H. Muta, K. Kurosaki, M. Uno, S. Yamanaka, *J. Alloys Compd.* **2006**, *420*, 25.